

Essential role of ALKBH5-mediated RNA demethylation modification in bile acid-induced gastric intestinal metaplasia

Ben Yue,^{1,6} Ran Cui,^{2,6} Ruizhe Zheng,^{3,6} Weilin Jin,⁴ Chenlong Song,⁵ Tianshang Bao,¹ Ming Wang,¹ Fengrong Yu,¹ and Enhao Zhao¹

¹Department of Gastrointestinal Surgery, Renji Hospital, School of Medicine, Shanghai Jiao Tong University, 160 Pujian Road, Shanghai 200127, China; ²Department of Hepatopancreatobiliary Surgery, Shanghai East Hospital, Tongji University School of Medicine, 1800 Yuntai Road, Shanghai 200120, China; ³Department of Neurosurgery, Tongren Hospital, School of Medicine, Shanghai Jiao Tong University, Shanghai 200336, China; ⁴Institute of Cancer Neuroscience, Medical Frontier Innovation Research Center, The First Hospital of Lanzhou University, The First Clinical Medical College of Lanzhou University, Lanzhou 730000, China; ⁵Department of General Surgery, Shanghai General Hospital, School of Medicine, Shanghai Jiao Tong University, 85 Wujin Road, Shanghai 200080, China

Bile acid reflux and subsequent caudal-related homeobox 2 (CDX2) activation contribute to gastric intestinal metaplasia (IM), a precursor of gastric cancer; however, the mechanism underlying this phenomenon is unclear. Here, we demonstrate that alkylation repair homolog protein 5 (ALKBH5), a major RNA N⁶-adenosine demethylase, is required for bile acid-induced gastric IM. Mechanistically, we revealed the N⁶-methyladenosine (m⁶A) modification profile in gastric IM for the first time and identified ZNF333 as a novel m⁶A target of ALKBH5. ALKBH5 was shown to demethylate ZNF333 mRNA, leading to enhanced ZNF333 expression by abolishing m⁶A-YTHDF2-dependent mRNA degradation. In addition, ALKBH5 activated CDX2 and downstream intestinal markers by targeting the ZNF333/CYLD axis and activating NF- κ B signaling. Reciprocally, p65, the key transcription factor of the canonical NF- κ B pathway, enhanced the transcription activity of ALKBH5 in the nucleus, thus forming a positive feedforward circuit. Furthermore, ALKBH5 levels were positively correlated with ZNF333 and CDX2 levels in IM tissues, indicating significant clinical relevance. Collectively, our findings suggest that an m⁶A modification-associated positive feedforward loop between ALKBH5 and NF- κ B signaling is involved in generating the IM phenotype of gastric epithelial cells. Targeting the ALKBH5/ZNF333/CYLD/CDX2 axis may be a useful therapeutic strategy for gastric IM in patients with bile regurgitation.

INTRODUCTION

Gastric intestinal metaplasia (IM), which replaces the gastric mucosa by epithelium-resembling intestinal morphology, is a well-recognized precancerous condition.¹ Patients with IM are at increased risk for gastric cancer (GC), with an estimated annual risk of 0.13%–0.25%/year.² As a precursor to intestinal-type GC, research on IM is imperative and fast growing.

Some chronic environmental stimulants, such as chronic infection with *Helicobacter pylori* and bile reflux, are considered drivers of IM.^{3,4} The effect of *Helicobacter pylori* infection on IM remains controversial.^{5,6} However, it is noteworthy that both gastric IM and Barrett's metaplasia of the esophagus, another type of IM, are the result of bile acid reflux.^{7,8} This strongly suggests a key regulatory role of bile acid reflux in IM.

The exact molecular mechanism responsible for bile acid-induced IM remains unclear. Accumulating evidence suggests a trigger effect of caudal-related homeobox 2 (CDX2) on IM.^{9,10} As an intestine-specific transcription factor, CDX2 promotes IM by upregulating the expression of Krüppel-like factor4 (KLF4), VILLIN (VIL1), and MUCIN 2 (MUC2).^{11,12} The expression of these genes is generally accepted as a hallmark of the IM process. The nuclear factor κ B (NF- κ B) pathway is also involved in this process.^{13,14}

N⁶-Methyladenosine (m⁶A), which is the most prominent chemical modification of RNA in eukaryotes, is a reversible and dynamic mark that regulates gene expression at the post-transcriptional level.¹⁵ In mammals, m⁶A modification is catalyzed by the m⁶A methyltransferases of methyltransferase-like 3 (METTL3), Wilms'

Received 4 April 2021; accepted 19 August 2021;
<https://doi.org/10.1016/j.omtn.2021.08.019>.

⁶These authors contributed equally

Correspondence: Enhao Zhao, PhD, Department of Gastrointestinal Surgery, Renji Hospital, School of Medicine, Shanghai Jiao Tong University, 160 Pujian Road, Shanghai 200127, China
E-mail: microzhaoenhao@hotmail.com

Correspondence: Fengrong Yu, PhD, Department of Gastrointestinal Surgery, Renji Hospital, School of Medicine, Shanghai Jiao Tong University, 160 Pujian Road, Shanghai 200127, China
E-mail: riry77@126.com

Correspondence: Ming Wang, PhD, Department of Gastrointestinal Surgery, Renji Hospital, School of Medicine, Shanghai Jiao Tong University, 160 Pujian Road, Shanghai 200127, China
E-mail: wangming1882@hotmail.com

tumor 1-associated protein (WTAP), and METTL14. Demethylation into adenosine occurs via alkylation repair homolog protein 5 (ALKBH5) or fat mass and obesity-associated factor (FTO).^{16–18} Recently, this newly discovered mechanism has been reported to play a critical role in regulating RNA fate, including mRNA stability and splicing, nuclear export, translation, microRNA processing and RNA-protein interactions,^{19–22} and is crucial for biological and disease processes, such as stemness maintenance and differentiation, fertility, stress response, immunomodulation, and tumorigenesis.^{23–26} We previously unveiled the METTL3-mediated m⁶A modification profile in GC for the first time and confirmed the dysregulation of m⁶A in the epithelial-mesenchymal transition (EMT) process and metastasis.²⁷ However, the definite role of m⁶A in gastric IM has never been studied.

In this study, we demonstrate that ALKBH5, an important demethyltransferase of RNA m⁶A modification, is a crucial regulator of the IM phenotype. Based on these results, we hypothesize that the ALKBH5-mediated m⁶A mechanism and downstream molecular changes may promote the process of bile acid-induced gastric IM.

RESULTS

Bile acids induce intestinal marker expression in gastric cells

Through preliminary experiments, peak levels of the key IM marker CDX2 were observed after the end of bile acid stimulation and replacement with normal medium for 48 h (Figures S1A and S1B). Therefore, to explore the possible effects of bile acids on the gastric IM process, we treated the gastric epithelial cell line GES-1 with three types of bile acids, namely, cholic acid (CA), deoxycholic acid (DCA), and chenodeoxycholic acid (CDCA) at different times or different doses after substituting normal medium for 48 h (Figure 1A). The IM phenotype was then determined by evaluating the expression of the intestinal markers CDX2, VIL1, and KLF4 by quantitative real-time-polymerase chain reaction (PCR). There was no significant difference in the expression of IM markers at each time point in cells without bile acid treatment (Figure S1C). We found that all three types of bile acids, particularly CDCA, induced the expression of intestinal markers in a time- and dose-dependent manner (Figures 1B and 1C). Therefore, CDCA was adopted as a powerful stimulus in subsequent experiments. In addition, treatment with CDCA resulted in an elevated expression of CDX2 at the protein level, as indicated by western blotting analysis. CDX2 has been reported to be highly expressed in the colon cancer cell lines LOVO and Caco2.^{28,29} We found that the expression of CDX2 in CDCA-treated GES-1 cells was comparable to that in LOVO and Caco2 cells (Figure S1D). These findings were further confirmed by confocal immunofluorescence microscopy (Figure 1D). Collectively, CDCA induced an IM phenotype in GES-1 cells.

ALKBH5 is required for gastric IM

We previously demonstrated that m⁶A modification promotes the EMT process of GC. Therefore, we next determined whether m⁶A plays a role in precancerous lesions. The expression of the major m⁶A-modification enzymes in gastric IM was explored using quanti-

tative real-time-PCR. As a result, ALKBH5 was significantly upregulated in GES-1 cells after treatment with CDCA (Figures 2A and 2B). According to the western blotting analysis, the expression of ALKBH5 positively correlated with CDX2 expression. Among the cell lines cultured, GES-1 and MGC803 cells expressed low levels of ALKBH5 and CDX2. By contrast, AGS cells showed a high expression of ALKBH5 and CDX2 (Figure 2C). To validate whether ALKBH5 is required for gastric IM, we performed loss- and gain-of-function studies and found that ALKBH5 overexpression caused a significant increase in expression of CDX2 and the downstream intestine-specific markers VIL1 and KLF4 in GES-1 and MGC803 cells (Figure 2D). However, knockdown of ALKBH5 led to the opposite result in AGS cells (Figure 2E). Interestingly, we observed that the depletion of ALKBH5 abolished the expression of gastric IM markers induced by CDCA (Figure 2F). Next, we measured ALKBH5 levels in the gastric IM tissue microarray (TMA) samples that included 80 cases (cohort 1) using immunohistochemistry (IHC). ALKBH5 immunoreactivity was predominantly positive in the majority of gastric IM specimens (Figure 2G). Among these tissues, 42 (52.5%) and 18 (22.5%) displayed strong and weak staining, respectively (Figure 2H). To further validate these results, we detected ALKBH5 expression in an additional 48 paired paraffin-embedded gastric IM tissues (cohort 2) and confirmed that ALKBH5 was significantly overexpressed in IM tissues as compared with adjacent normal gastric tissues (Figures 2I and 2J). Overall, these data indicate that ALKBH5 facilitates gastric IM induced by bile acids.

ZNF333 is a direct target of ALKBH5 in bile acid-induced gastric IM

To identify the transcripts regulated by m⁶A, we profiled m⁶A distribution at the transcriptome level in control or CDCA-treated GES-1 cells through m⁶A sequencing. Similar overall m⁶A patterns were observed in the two cell groups (Figures 3A and 3B; Figures S2A and S2B). Similarly, no significant difference in total m⁶A levels was observed between the control and CDCA-treated GES-1 cells (Figure 3C). Next, we analyzed the m⁶A-sequencing data. In total, m⁶A-sequencing identified 63,093 and 52,188 m⁶A peaks in the control and CDCA-treated cells, respectively (Figure 3D; Figures S2C and S2D). In contrast to the unique peaks observed in the control (49.6%) and treated (39.0%) groups, 11.4% peaks were found in both groups (Figure 3E). When m⁶A methylomes were mapped, the m⁶A consensus motif of GGAC (RRACH) was found to be highly enriched within m⁶A sites (Figure 3F). As ALKBH5 is an RNA demethylase, we focused on m⁶A peaks with diminished sizes. In GES-1 cells treated with CDCA, 2,994 peaks were found to be diminished (Figure 3G). We found that the differentially expressed m⁶A-modified transcripts were involved in nucleic acid binding, catalytic activity, DNA binding, pathways in cancer, metabolic pathways, cell cycle, and RNA transport (Figures S2E and S2F). To compare the gene expression profile following CDCA treatment in GES-1 cells, RNA-sequencing analysis was performed. A total of 1,818 transcripts were differentially expressed ($|\log_2(\text{fold change})| > 1$) (Figure 3H; Table S1). Next, we ascertained whether these altered transcripts were a consequence of m⁶A modification. It has been reported that ALKBH5 demethylates

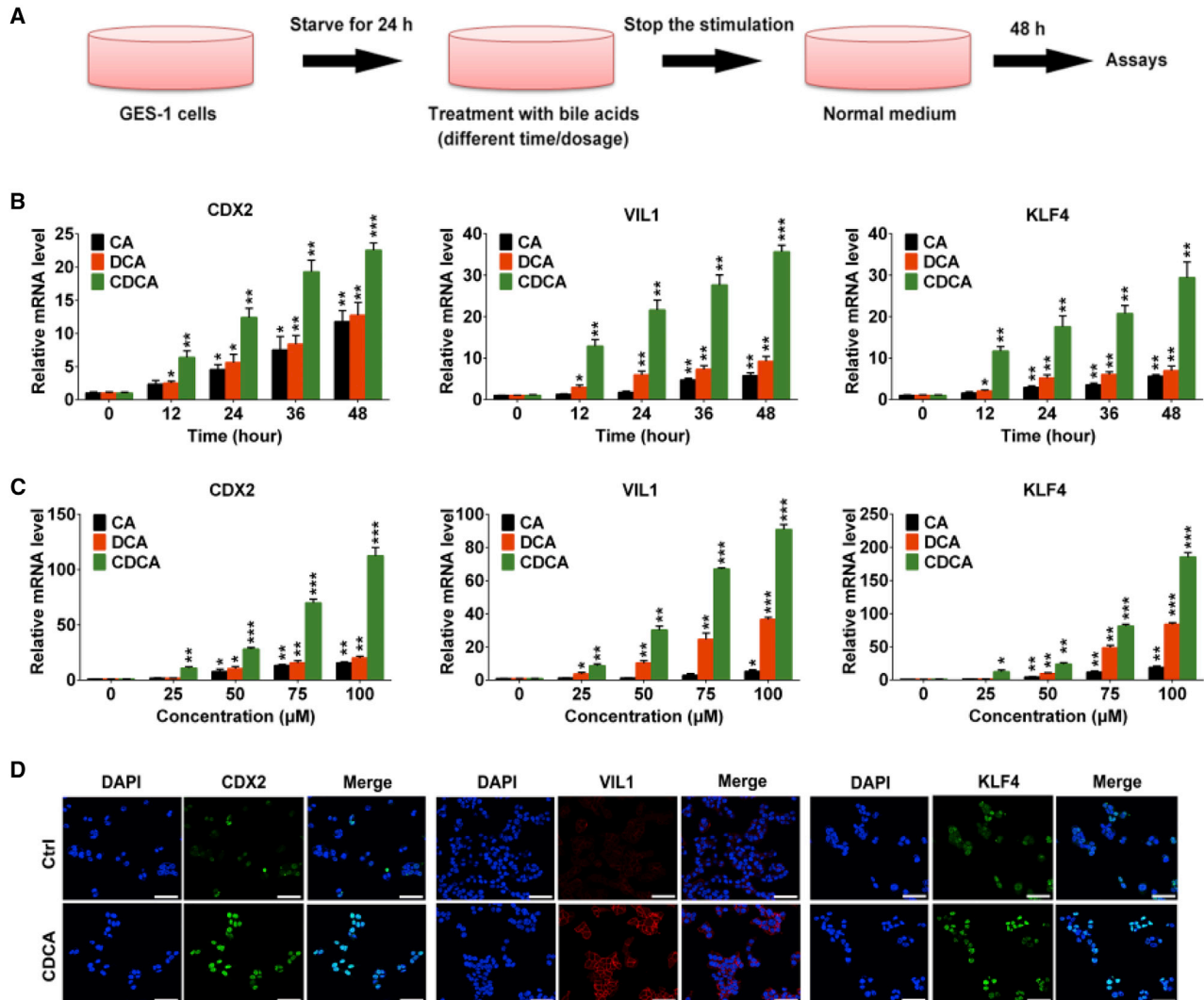


Figure 1. Bile acids induce intestinal metaplasia (IM) phenotype in gastric cells

(A) The gastric epithelial cell line GES-1 was treated with bile acids to establish an IM model. (B) The expression of CDX2, VIL1, and KLF4 were increased following bile acids treatment in a time-dependent manner. Time point: 12, 24, 36, and 48 h at 50 μM . (C) The expression of CDX2, VIL1, and KLF4 were increased following bile acids treatment in a dose-dependent manner. Dosage: 25, 50, 75, and 100 μM for 24 h. (D) The localization and expression of CDX2, VIL1, and KLF4 were confirmed by confocal immunofluorescent assay in GES-1 cells treated with 100 μM CDCA for 48 h. Scale bars: 50 μm . Each experiment was performed in triplicate. * $p < 0.05$, ** $p < 0.01$, *** $p < 0.001$.

the target mRNA, leading to enhanced transcript expression.^{30,31} Thus, elevated transcripts with diminished m^6A levels were selected in our study. Filtering the 2,994 diminished m^6A peaks with the 644 elevated transcripts resulted in the identification of 27 peaks harbored by 24 transcripts (Figure 3G). Importantly, the m^6A modification of 6 gene transcripts—LIPT1, ZMYM5, ZNF333, DICER1-AS1, ARRDC3-AS1 and LOC101927497—was decreased by >9-fold (Table S2). Among these genes, a sharp decrease in the size of the m^6A peaks was detected around the exon of ZNF333 mRNA (chr19: 14829096-14829367) in CDCA-treated cells as compared to the control (Figure 3I), and the expression of ZNF333 increased in

response to CDCA (Figure 3J). Intriguingly, ZNF333 mRNA levels were abolished by the inhibition of ALKBH5 (Figure 3K). Thus, ZNF333 may be a direct target of ALKBH5 and was selected for the subsequent study on CDCA-induced IM.

ALKBH5 maintains ZNF333 expression in gastric IM

To further characterize the regulation of ZNF333 expression by ALKBH5, quantitative real-time-PCR and western blotting analyses were performed. Both GES-1 and MGC803 cells with ectopic expression of ALKBH5 exhibited an increase in ZNF333 at both the mRNA and protein levels (Figures 4A–4C). Reciprocally,

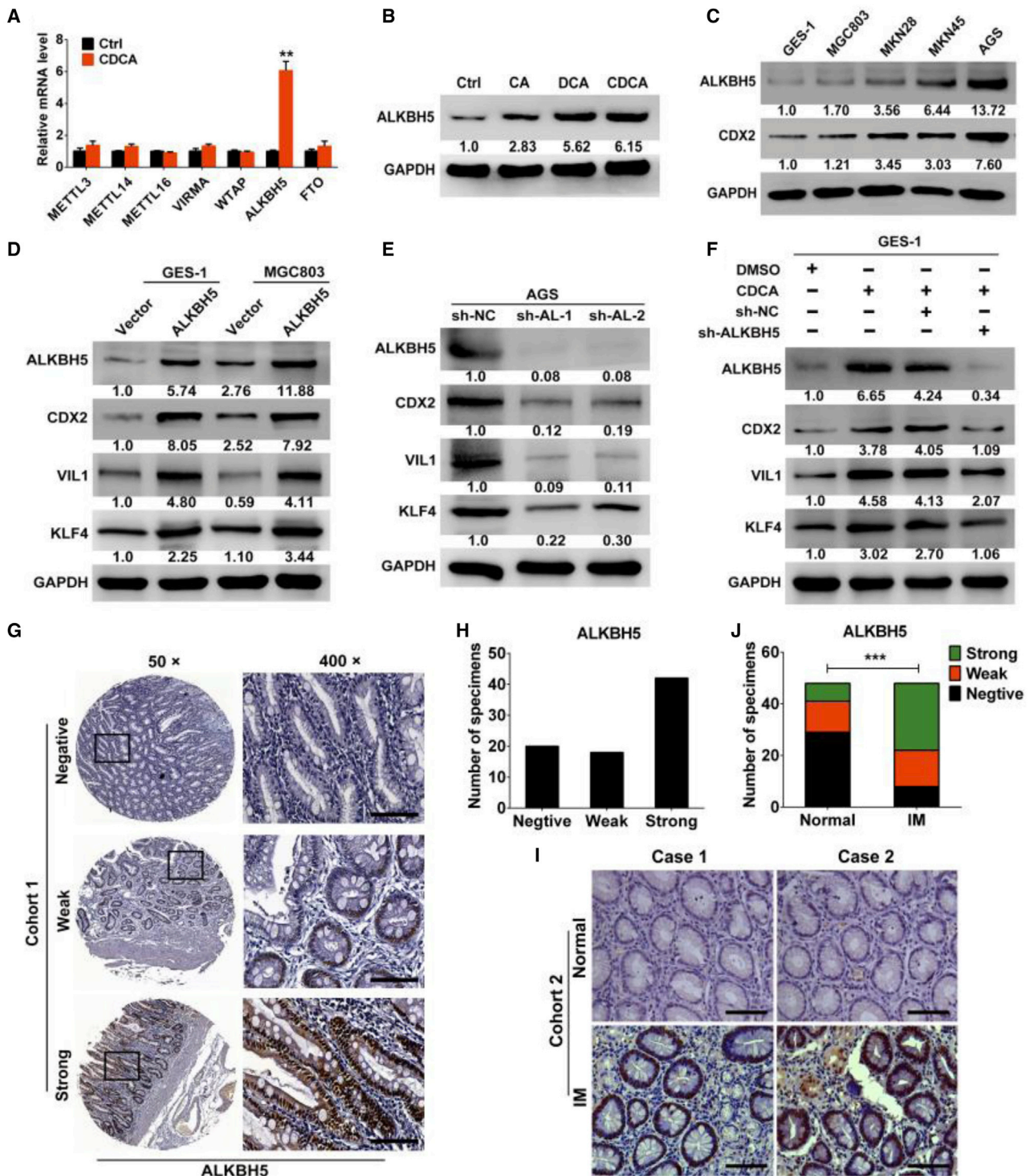


Figure 2. Gain of IM features correlates with ALKBH5 expression

(A) ALKBH5 was upregulated significantly in response to 100 μ M CDCA treatment for 48 h evaluated by quantitative real-time-PCR in GES-1 cells. (B) ALKBH5 expression was determined by western blot in GES-1 cells treated with different types of bile acids. (C) Western blot analysis of ALKBH5 and CDX2 in different cell lines. (D and E)

(legend continued on next page)

knockdown of ALKBH5 reduced ZNF333 expression in AGS cells (Figures 4D and 4E). Through immunofluorescence analysis, we identified the nuclear colocalization of ALKBH5 and ZNF333 in cells in which overexpression of ALKBH5 upregulated ZNF333 levels, whereas depletion of ALKBH5 mediated the loss of ZNF333 (Figures 4F and 4G). In addition, CDCA induced immunofluorescence staining of ZNF333 in GES-1 cells, which was abrogated by the introduction of sh-ALKBH5 lentiviral transduction (Figure 4H). We also validated ZNF333 expression in the IM TMA (cohort 1). Based on the results of immunohistochemical serial section staining, the level of ZNF333 co-expressed with ALKBH5, was frequently elevated in gastric IM tissues (Figures 4I and 4J). These data revealed that ALKBH5 positively regulates ZNF333 expression in gastric IM.

ALKBH5 increases ZNF333 expression by abolishing m⁶A-YTHDF2-dependent mRNA degradation

To reveal the m⁶A-related regulatory mechanism of ZNF333 expression by ALKBH5, we validated the m⁶A-sequencing data using m⁶A methylated RNA immunoprecipitation (MeRIP) quantitative real-time-PCR. The m⁶A-specific antibody dramatically reduced the enrichment of ZNF333 mRNA upon ALKBH5 overexpression (Figure 5A) while remarkably increasing the enrichment of ZNF333 mRNA levels upon ALKBH5 knockdown (Figure 5B). In addition, unlike wild-type ALKBH5, the catalytically inactive mutant ALKBH5 overexpression could not regulate ZNF333 expression at both the mRNA and protein levels (Figures 5C–5F). Moreover, increased expression of ZNF333 mRNA was observed when the global methylation inhibitor 3-deazaadenosine (DAA) was introduced (Figure 5G). These findings suggest that ALKBH5 mainly modulates ZNF333 expression through its demethylation activity. The function of m⁶A in modulating RNA expression is executed mostly by the reader proteins.³² Recent evidence has demonstrated the regulation of YTHDF2 on the targets of ALKBH5.³¹ As expected, the YTHDF2 binding site was close to the m⁶A modification region of ZNF333 as revealed by our m⁶A-sequencing (Figure 5H). We found that the overexpression of YTHDF2 partially counteracted the effects of elevated ALKBH5 levels on the expression of ZNF333 at both mRNA and protein levels in GES-1 cells (Figures 5I and 5J). Conversely, the reduced expression of ALKBH5 decreased ZNF333 expression, and inhibition of YTHDF2 reversed this decrease in AGS cells (Figures 5K and 5L) and CDCA-treated GES-1 cells (Figures S3A and S3B). Furthermore, knockdown of ALKBH5 weakened the stability of ZNF333 mRNA, whereas knockdown of YTHDF2 strengthened the stability of ZNF333 mRNA in sh-ALKBH5 cells (Figure 5M). These results suggest that YTHDF2-mediated RNA decay controls the expression of ZNF333. In other words, ALKBH5 increases ZNF333 expression by abolishing m⁶A-YTHDF2-dependent mRNA degradation.

ALKBH5 regulates gastric IM through a ZNF333-NF-κB pathway

To obtain a better understanding of the potential regulatory role of the ALKBH5/ZNF333 axis in gastric IM, we performed RNA sequencing to analyze the gene expression profile affected by the overexpression of ZNF333 and found 460 dysregulated genes in the treated cells as compared with the control (Figures 6A and 6B). Kyoto Encyclopedia of Genes and Genomes (KEGG) pathway analysis showed that the NF-κB, p53, vascular endothelial growth factor (VEGF), and mitogen-activated protein kinase (MAPK) pathways were significantly enriched in ZNF333 overexpressing cells (Figure 6C). A pathway reporter array that included the aforementioned signaling pathways was used for further validation. The results showed that NF-κB signaling was significantly activated by ZNF333 (Figure 6D). Further studies revealed that silencing ALKBH5 reduced the expression of ZNF333 and phosphorylation of p65, while the inhibition of p65 phosphorylation by Bay, a specific inhibitor of NF-κB signaling, decreased the expression of gastric IM markers induced by ALKBH5 (Figures 6E and 6F). In addition, the role of ALKBH5 in promoting the redistribution of p65 to nuclear localization was confirmed by confocal immunofluorescence assays (Figures 6G and 6H; Figures S4A and S4B). To determine whether the effects of ALKBH5 on NF-κB signaling and gastric IM were specifically attributed to the ALKBH5/ZNF333 axis, GES-1 cells were transduced with lentiviruses carrying ALKBH5 and/or sh-ZNF333, and AGS cells were transduced with lentiviruses carrying sh-ALKBH5 and/or ZNF333. Western blotting analysis showed that knockdown of ZNF333 partly counteracted the activation of NF-κB signaling and the acceleration of the IM phenotype caused by ALKBH5 overexpression (Figure 6I). In contrast, elevation of ZNF333 expression recapitulated the levels of phosphorylated (p-) p65 and gastric IM markers in sh-ALKBH5 cells (Figure 6J). In addition, through a luciferase reporter assay, we observed that CDCA treatment activated NF-κB signaling, which was repressed by the depletion of ALKBH5 or ZNF333 (Figure 6K). These results demonstrate a bile acid-induced gastric IM process involving the ALKBH5/ZNF333/NF-κB signaling axis.

ZNF333/CYLD axis activates NF-κB pathway and CDX2 expression

As the largest transcription factor family in the human genome, zinc finger proteins exhibit a wide variety of functions involving transcriptional activation or repression effects.^{33,34} Thus, we assessed the transcriptional activity of ZNF333 by fusing its full length to the DNA-binding domain of Gal4 in GES-1 and AGS cells (Figure 7A). Using the Gal4-driven luciferase reporter system, we found that ZNF333 markedly repressed reporter activity in a dose-dependent manner (Figures 7B and 7C). In addition, the overexpression of FLAG-ZNF333 did not influence the activity of the Gal4-driven reporter (Figure S5A), demonstrating that ZNF333 physically binds to DNA to exert its transcriptional repressive function.

ALKBH5 overexpression or knockdown influenced the expression levels of IM markers in the western blot assay. (F) The expression of gastric IM markers was determined by quantitative real-time-PCR in GES-1 cells treatment with CDCA (100 μM for 48 h) and/or transfected with lentiviruses carrying sh-ALKBH5. Each experiment was performed in triplicate. (G and H) Representative images of IHC staining for ALKBH5 protein on a TMA constructed from 80 gastric IM tissues (cohort 1). (I and J) The levels of ALKBH5 in 48 gastric IM tissues and paired normal tissues (cohort 2) were determined by IHC staining. Scale bars: 100 μm. **p < 0.01, ***p < 0.001.

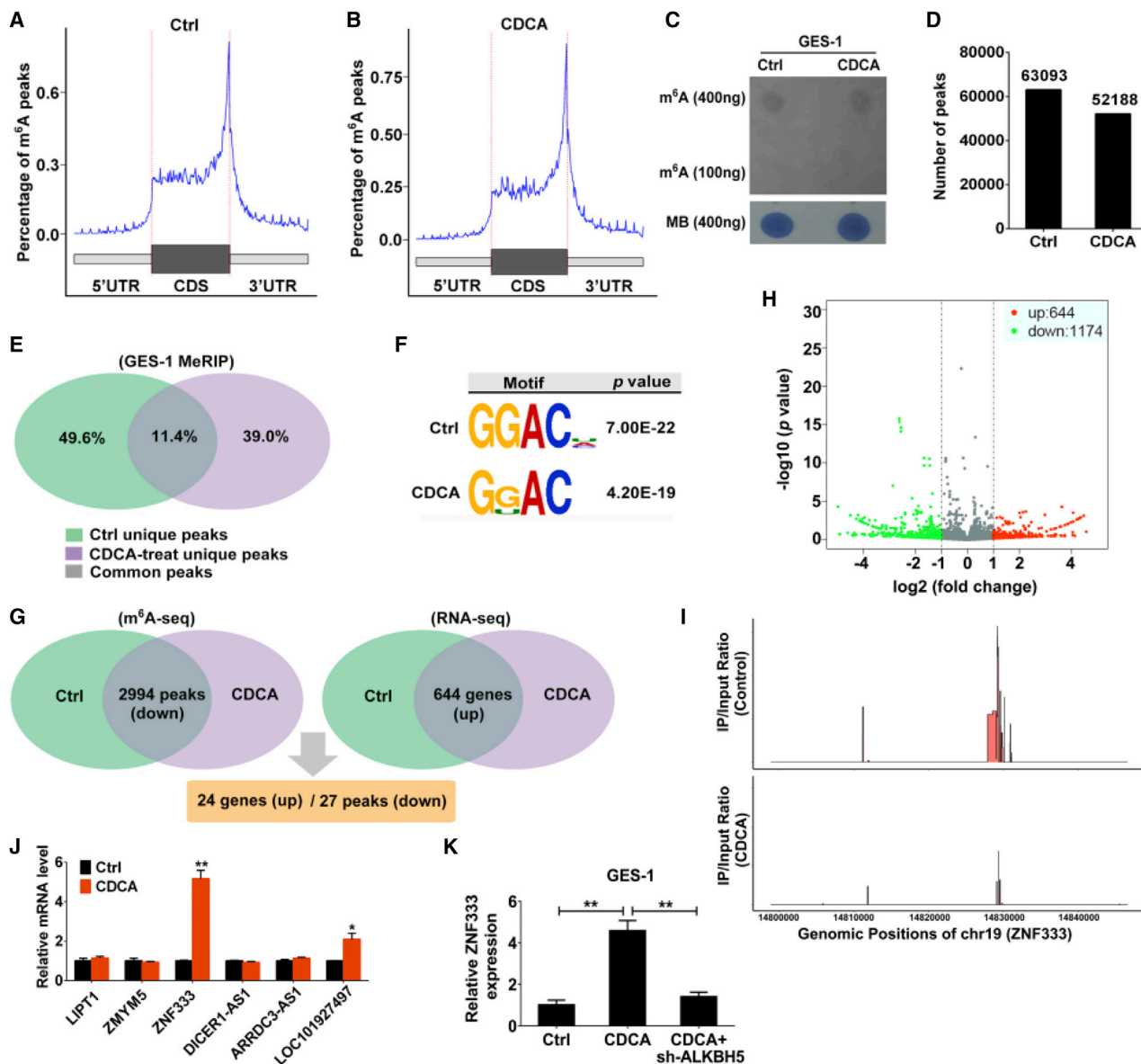


Figure 3. Identification of potential target of ALKBH5 in bile acid-induced gastric IM

(A and B) Similar overall m⁶A patterns were observed in control or CDCA-treated GES-1 cells. Incubating dosage: 100 μ M, time: 48 h. (C) m⁶A dot blot assay was performed in control or CDCA-treated GES-1 cells. MB, methylene blue. (D) Number of m⁶A peaks in control and CDCA-treated cells. (E) Number of common or unique m⁶A peaks identified in m⁶A sequencing in control and CDCA-treated cells. (F) Top consensus motif identified by HOMER with m⁶A sequencing peaks in GES-1 cells with or without CDCA treatment. (G) Filtering the diminished m⁶A peaks with the upregulated genes in CDCA-treated GES-1 cells identified the potential direct targets of ALKBH5. (H) RNA sequencing was performed in CDCA-treated GES-1 cells as compared with the control. (I) Treatment with CDCA diminishes m⁶A modification of ZNF333 mRNA in GES-1 cells. (J) The mRNA level of ZNF333 was mostly increased in CDCA-treated cells (100 μ M for 48 h) compared to the control. (K) The expression of ZNF333 was determined by quantitative real-time-PCR in GES-1 cell treatment with CDCA (100 μ M for 48 h) and/or transfected with lentiviruses carrying sh-ALKBH5. **p < 0.01.

ZNF333 recognizes the consensus binding site ATAAT (Figure S5B).³⁵ We searched the human genome with the motif for ZNF333 using Find Individual Motif Occurrences (FIMO), a software tool for scanning DNA or protein sequences with motifs described as position-specific scoring matrices,³⁶ and identified a potential binding site on the promoter of CYLD (in the range of -952 to -944 bp),

which negatively regulates the NF- κ B pathway by inhibiting the IKK complex.^{37,38} Chromatin immunoprecipitation (ChIP) assays verified that ZNF333 directly binds to this region of the CYLD promoter (Figures S5C and S5D). To explore the correlation between the ZNF333/CYLD axis and NF- κ B pathway, we conducted an immunofluorescence assay and confirmed that elevated levels of

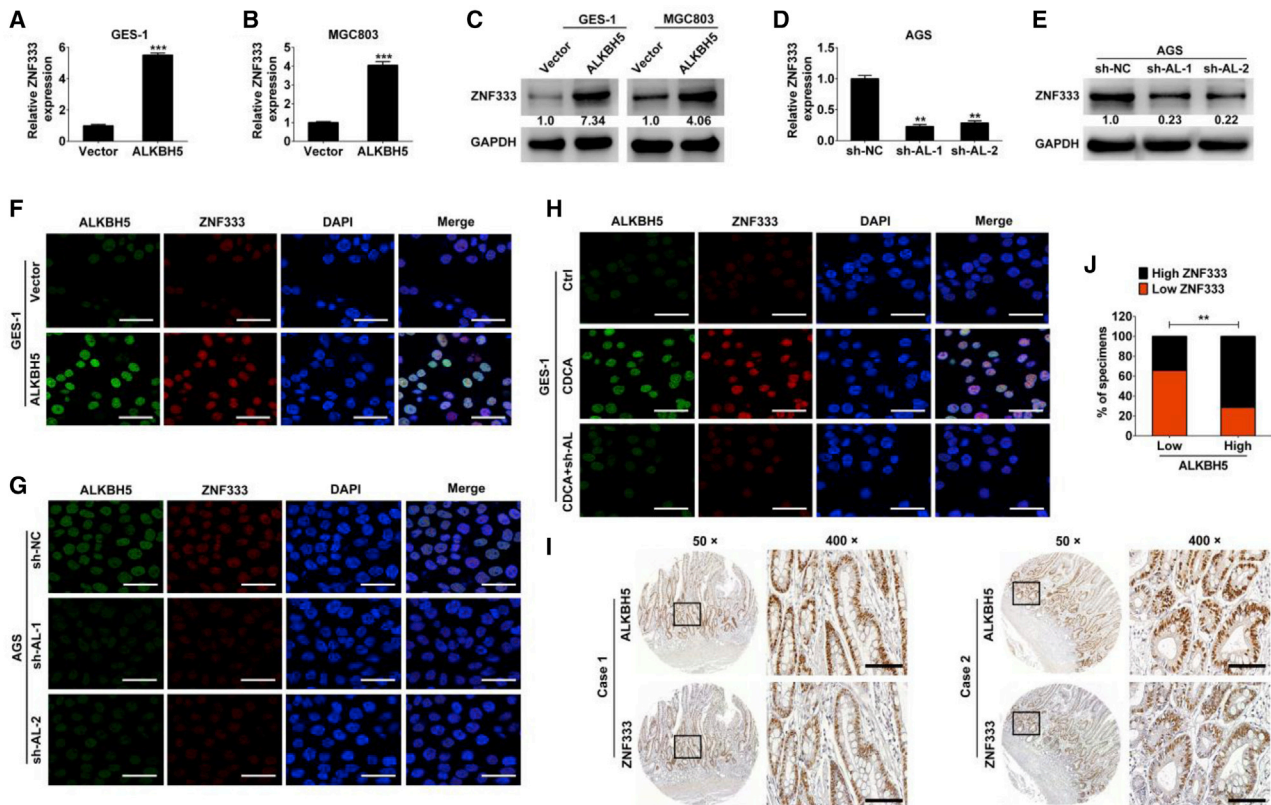


Figure 4. ALKBH5 maintains ZNF333 expression in gastric IM

(A–C) ZNF333 expression upon ALKBH5 overexpression as measured by quantitative real-time-PCR and western blot. (D and E) ZNF333 expression upon ALKBH5 knockdown as measured in AGS cells. (F and G) Co-expression of ALKBH5 and ZNF333 in GES-1 and AGS cells were determined by confocal immunofluorescent assay. Scale bars: 50 μ m. (H) Co-expression of ALKBH5 and ZNF333 was determined by confocal immunofluorescent assay in GES-1 cell treatment with CDCA (100 μ M for 48 h) and/or transfected with lentiviruses carrying sh-ALKBH5. Scale bars: 50 μ m. Each experiment was performed in triplicate. (I and J) Representative IHC staining of ZNF333 in pathologic serial sections of IM tissues with low or high ALKBH5 expression. Scale bars: 100 μ m. ** p < 0.01, *** p < 0.001.

CYLD significantly inhibited the nuclear translocation of p65 upon stimulation with tumor necrosis factor α (TNF- α) (Figure S5E). Further studies revealed that ectopic expression of ZNF333 resulted in decreased mRNA and protein levels of CYLD, whereas knockdown of ZNF333 increased CYLD levels (Figures 7D–7F). In addition, silencing CYLD or overexpression of ZNF333 activated NF- κ B signaling and the downstream targets, which were considerably attenuated by the restoration of CYLD (Figures 7G and S5F–S5H). These data demonstrate that ZNF333 promotes canonical NF- κ B signaling via transcriptional repression of CYLD. We further revealed that CDX2 was positively correlated with the expression of p-p65 in 48 gastric IM tissues (cohort 2) (Figures 7H and 7I), consistent with recent studies.^{12,39} Bioinformatics analysis of the promoter region of CDX2 by JASPAR (jaspar.genereg.net) predicted a DNA-binding element for p65 (Figure 7J). A ChIP assay confirmed that the enrichment of p65 in this region was considerably increased in GES-1 cells treated with CDCA (Figure 7K). These results suggest that the ZNF333/CYLD axis mediates the upregulation of NF- κ B signaling transcriptionally activated CDX2 in CDCA-stimulated gastric cells.

p65-mediated activation of ALKBH5 transcription in gastric IM

Accumulating evidence has shown that functional feedforward circuits are involved in biological processes.⁴⁰ Intriguingly, in our preliminary exploration, ALKBH5 expression was markedly increased when NF- κ B signaling was activated by using a specific signaling activator TNF- α . Conversely, Bay, which is an inhibitor of NF- κ B signaling, repressed the levels of ALKBH5 (Figures 7L–7N). These clues inspired us to speculate on a possible feedforward loop between ALKBH5 and NF- κ B signaling. To validate our hypothesis, a series of luciferase reporter plasmids containing the truncated ALKBH5 promoter were transfected into CDCA-treated GES-1 cells. The results showed that CDCA-mediated ALKBH5 regulation was controlled by putative NF- κ B binding sites (Figure 7O). The ChIP assay confirmed that p65 directly bound to the 2 regions (–673 to –664 bp and –1314 to –1305 bp). In addition, the anti-p65 antibody dramatically enriched ALKBH5 expression in cells treated with CDCA compared to the control (Figures 7P and 7Q). These data suggest that p65 binds to the ALKBH5 promoter and accelerates ALKBH5 transcription, thus forming a positive feedback loop in bile acid-induced gastric IM.

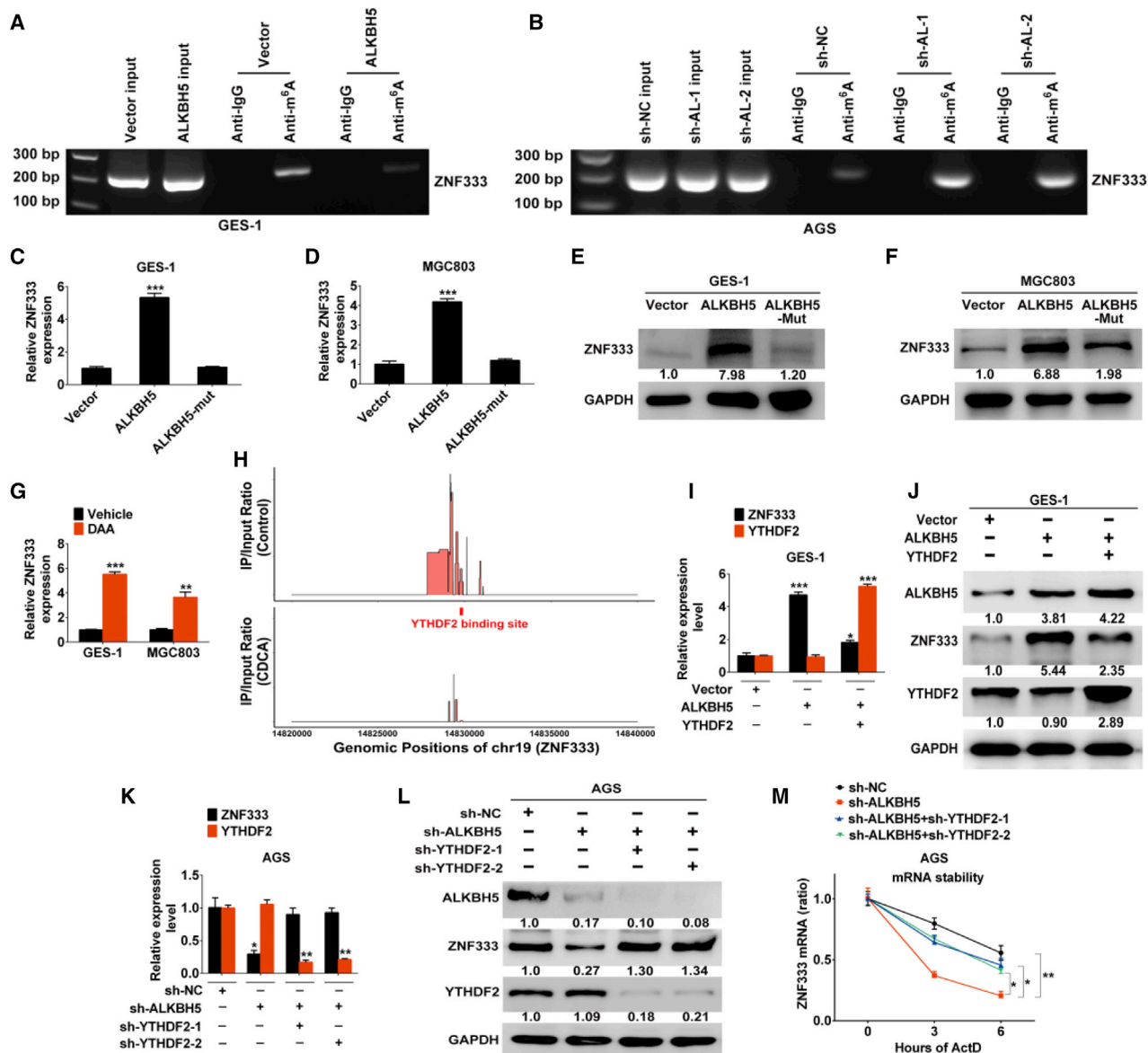


Figure 5. ALKBH5 regulates ZNF333 expression through suppressing m⁶A/YTHDF2-mediated mRNA decay

(A and B) RIP with anti-m⁶A antibody was performed in GES-1 and AGS cells. m⁶A demethylation modification on ZNF333 was enhanced by ALKBH5 overexpression, whereas it was depleted upon ALKBH5 knockdown. (C and D) The mRNA levels of ZNF333 were measured via quantitative real-time-PCR in wild-type or catalytic mutant ALKBH5-overexpressing cells. (E and F) Western blotting of ZNF333 in cells transfected with control, wild-type, or mutant ALKBH5 plasmid. (G) The mRNA levels of ZNF333 were measured in both GES-1 and MGC803 cells after treatment with 3-deazaadenosine (DAA). (H) m⁶A sequencing identification of m⁶A modification in ZNF333 mRNA near the YTHDF2 binding site. (I and J) ZNF333 and YTHDF2 expressions were examined by quantitative real-time-PCR and western blot in GES-1 cells transfected with lentiviruses carrying ALKBH5 and/or YTHDF2. (K and L) ZNF333 and YTHDF2 expression were examined by quantitative real-time-PCR and western blot in AGS cells transfected with lentiviruses carrying sh-ALKBH5 and/or sh-YTHDF2. (M) qPCR analysis of the mRNA stability of ZNF333 in AGS cells with or without ALKBH5 knockdown in combination with or without knockdown of YTHDF2. Each experiment was performed in triplicate. *p < 0.05, **p < 0.01, ***p < 0.001.

ALKBH5/ZNF333/CDX2 pathway is characteristic of IM tissues

To evaluate the clinical relevance of the signaling axis previously described, 48 pairs of gastric IM tissues (cohort 2) were used for further immunohistochemical staining (Figure 8A). Elevated expression of ALKBH5, ZNF333, and CDX2 was observed, with a concur-

rent low level of CYLD in gastric IM tissues as compared with adjacent normal mucosa (Figures 8B–8E). The IM cases were then divided into high and low groups based on the expression of ALKBH5, ZNF333, CYLD, and CDX2. As expected, ALKBH5 expression was positively correlated with ZNF333 and CDX2 and negatively

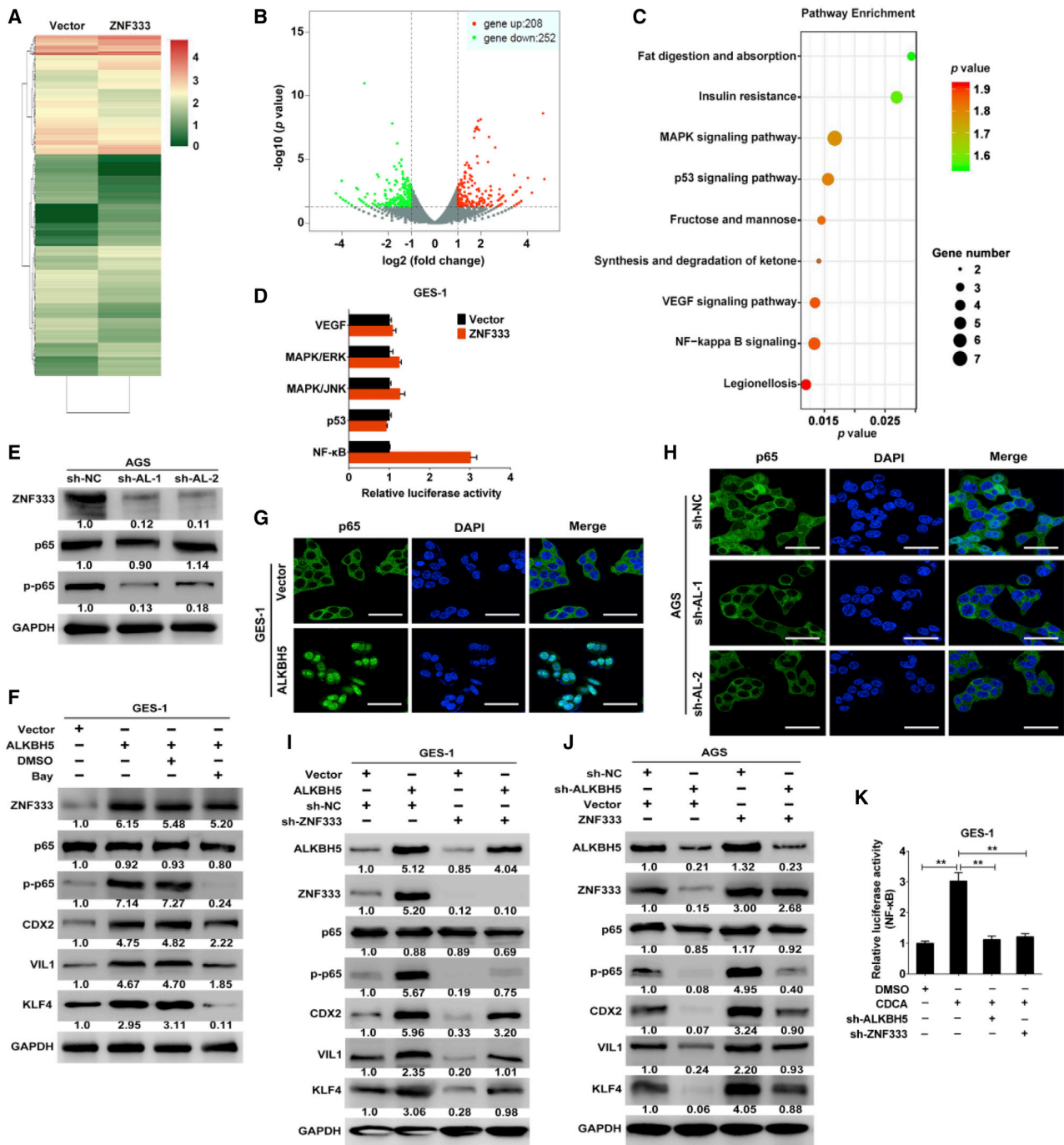


Figure 6. ALKBH5 regulates gastric IM through a ZNF333-NF-κB pathway

(A and B) RNA sequencing was performed in GES-1 cells with or without ZNF333 overexpression. In the heatmap, numbers 1–4 represent the color scale: 1–2 represents the color from dark green to light green, 3–4 represents the color from orange to red. Red: increased expression, green: decreased expression. (C) KEGG pathway analysis in GES-1 cells with ZNF333 overexpression. (D) Signaling pathway reporter array was carried out for seeking the relative pathway associated with ZNF333. (E) The levels of ZNF333, p65, and p-p65 were detected by western blot in AGS cells with or without ALKBH5 knockdown. (F) The levels of p-p65 and IM markers were examined by western blot in GES-1 cells with ALKBH5 overexpression together with dimethylsulfoxide (DMSO) or NF-κB signaling inhibitor Bay (1 μM). (G and H) The role of ALKBH5 in promoting the redistribution of p65 to nuclear localization was confirmed via immunofluorescence assay. Scale bars: 50 μm. (I) The protein levels of p-p65 and IM markers were

(legend continued on next page)

correlated with CYLD expression (Figures 8F–8H). Finally, another 20 pairs of gastric IM tissues (cohort 3) were collected and identified (Figure 8I). To further support the results of cohort 2, we extracted RNA from cohort 3 and performed quantitative real-time-PCR assays. Similarly, the mRNA levels of ALKBH5, ZNF333, and CDX2 were upregulated in gastric IM tissues, whereas CYLD mRNA levels were significantly decreased (Figures 8J–8M). ALKBH5 transcript levels were co-expressed with ZNF333 and CDX2 mRNA levels. Reciprocally, an inverse correlation was observed between ALKBH5 and CYLD at the mRNA level (Figures 8N–8P). Overall, these findings suggest that the ALKBH5/ZNF333/CDX2 pathway is responsible for human gastric IM (Figure 8Q).

DISCUSSION

Bile reflux is considered a precursor of gastric IM. Currently, the expression of CDX2 and its downstream intestinal markers are generally accepted as hallmarks of the IM process.¹¹ To clarify the precise mechanism of transformation to IM in gastric epithelium, we successfully established an IM model in the normal gastric epithelial cell line GES-1 through the stimulation of bile acids, which was consistent with previous studies.¹² The latest evidence indicates that m⁶A modulators, including “writers” (METTL3, METTL14, KIAA1429, and WTAP), “readers” (YTHDF1/2/3, YTHDC1, eIF3, and HNRNPA2B1), and “erasers” (ALKBH5 and FTO) have critical and diverse functions in physiological and pathological processes.⁴¹ However, the dysregulation of m⁶A in human IM remains unclear. Here, we filled this gap with studies confirming the upregulation of the m⁶A modulator ALKBH5 in bile acid-induced gastric IM. ALKBH5-mediated m⁶A demethylation-maintained mRNA stability and thus could increase transcript levels.³⁰ In the present study, based on the RNA and m⁶A sequencing experiments, we filtered the candidate transcripts and identified ZNF333 as a downstream target of ALKBH5-mediated m⁶A modification in gastric cells with an intestine-like phenotype, which was further confirmed by MeRIP. We found that the epigenetic regulation of ZNF333 by ALKBH5 appeared to be mediated by abolishing m⁶A-YTHDF2-dependent mRNA degradation, because (1) knockdown of ALKBH5 decreased the mRNA level and stability of ZNF333; (2) the binding site of the m⁶A reader YTHDF2 was close to the m⁶A modification region in ZNF333; (3) knockdown of YTHDF2 increased the mRNA level and stability of ZNF333, thus reversing the effect of ALKBH5 knockdown; and (4) overexpression of YTHDF2 decreased the mRNA levels of ZNF333, attenuating the effect of elevated ALKBH5 expression. In addition, Gene Ontology (GO) and KEGG analyses of m⁶A sequencing showed the enrichment of some biological processes beyond our knowledge in bile acid-treated cells as compared with the control, indicating the possible involvement of other m⁶A mechanisms in gastric IM.

ZNF333 is a member of a subfamily of zinc finger proteins with a molecular weight of 75.5 kDa and is localized on chromosome 19p13.1. Despite the transcriptional repressive ability of ZNF333, as previously reported, its function has been unknown until now.⁴² In the present study, ectopic expression of ZNF333 was detected in bile acid-induced gastric IM. Its transcriptional repressive activity was confirmed using the luciferase reporter system. Moreover, by means of KEGG pathway analysis of the transcriptome-sequencing data, we identified the enrichment of NF- κ B signaling in ZNF333-overexpressing cells and further showed evidence that ALKBH5-mediated m⁶A demethylation in epigenetic activation of ZNF333 transcription represses CYLD, thus accelerating NF- κ B signaling. We also observed NF- κ B-mediated CDX2 transcriptional activation in gastric IM, which was consistent with recent studies.⁴³ Accumulating studies have demonstrated the existence of functional feedforward loops. The expression of ALKBH5 was upregulated or downregulated by the introduction of an NF- κ B signaling activator or inhibitor in GES-1 cells, respectively, strongly implying that this loop mechanism is involved. As expected, the transcriptional activation of ALKBH5 by NF- κ B was validated using luciferase reporter and ChIP assays. Finally, we identified the active ALKBH5/ZNF333/CYLD/CDX2 pathway in gastric IM tissues, indicating its clinical significance.

In our study, CDCA treatment largely increased ALKBH5 expression but did not alter the expression of other major m⁶A-modification enzymes, such as METTL3, METTL14, METTL16, FTO, and WTAP. Presumably, the increase in ALKBH5 expression could alter the total m⁶A levels or distribution. However, there was no difference in total m⁶A RNA and overall m⁶A patterns between the control and CDCA-treated groups. The possible explanation for this is as follows: on the one hand, while protein levels of ALKBH5 are significantly upregulated, its enzyme activity may not be enough to cause changes in total m⁶A levels; on the other hand, the m⁶A process is dynamic and reversible. Whether other potential m⁶A modification enzymes or novel modulators compensate for their roles when ALKBH5 is genetically upregulated in bile acid-induced gastric cells remains uncertain. Thus, an interesting and significant future study is needed to further determine their potential modulation.

We identified that an m⁶A-associated positive feedforward loop between ALKBH5 and NF- κ B signaling is involved in IM development. To the best of our knowledge, this is the first study to elucidate the m⁶A modification profile in human gastric IM. The newly identified ALKBH5/ZNF333/NF- κ B pathway further improves the currently hypothesized mechanism underlying the regulation of CDX2 and provides several new insights into the early detection and prevention of GC. Targeting ALKBH5 and ZNF333 may be a useful preventive and therapeutic strategy for gastric IM in patients with bile regurgitation and therefore may have great value for clinical transformation.

measured by western blot analysis in GES-1 cells transfected with lentiviruses carrying ALKBH5 and/or sh-ZNF333. (J) The protein levels of p-p65 and IM markers were measured by western blot analysis in AGS cells transfected with lentiviruses carrying sh-ALKBH5 and/or ZNF333. (K) CDCA (100 μ M for 48 h) treated GES-1 cells infected with lentiviruses carrying sh-ALKBH5 and/or sh-ZNF333, along with transfected with a NF- κ B-luciferase reporter vector. Then, Luciferase reporter assay was performed to measure the NF- κ B-luciferase activity. Each experiment was performed in triplicate. **p < 0.01.

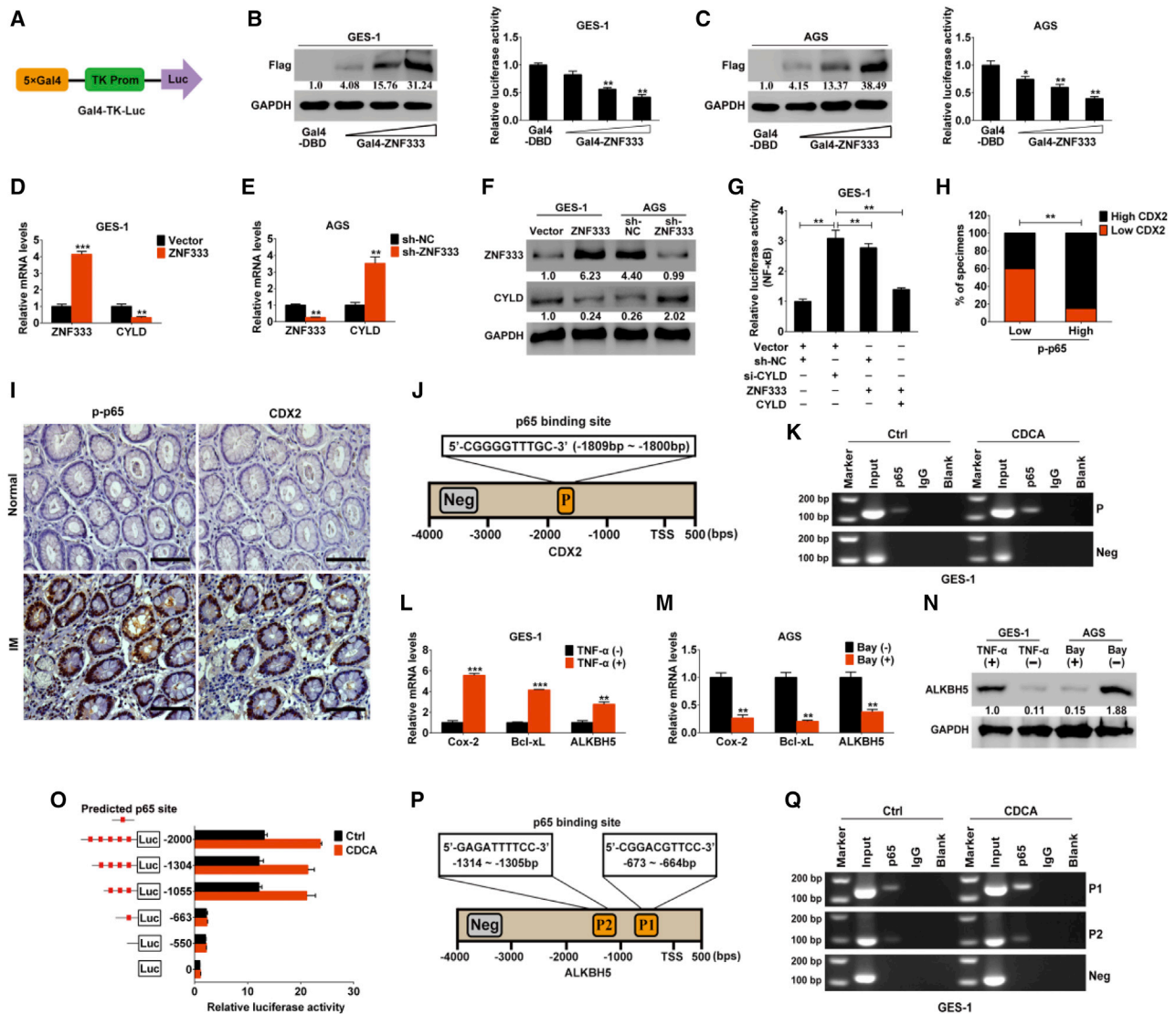


Figure 7. The positive feedforward loop between ALKBH5 and NF- κ B signaling in gastric IM

(A) The schematic diagram showing the Gal4-luciferase reporter. (B and C) GES-1 and AGS cells were transfected with different amounts of Gal4-ZNF333 expression plasmids together with the Gal4-luciferase reporter. Luciferase reporter assay was performed after 48 h. (D and E) ZNF333 and CYLD transcripts upon ZNF333 overexpression or knockdown were measured by quantitative real-time-PCR. (F) ZNF333 and CYLD protein levels upon ZNF333 overexpression or knockdown were measured by western blotting analysis. (G) Luciferase reporter assay was performed to detect the signaling activity in GES-1 cells transfected with the NF- κ B-luciferase reporter, along with si-CYLD and/or ZNF333 and/or CYLD. (H) Association between p-p65 and CDX2 levels in 48 gastric IM tissues (Cohort 2). (I) The representative images of IHC staining for p-p65 and CDX2 in pathologic serial sections of gastric IM tissues and paired normal tissues. Scale bars: 100 μ m. (J and K) p65 bound specifically to the CDX2 promoter in GES-1 cells. (L–N) ALKBH5 expression was measured in GES-1 cells treated with 10 ng/mL TNF- α for 24 h or in AGS cells treated with 1 μ M Bay for 24 h by quantitative real-time-PCR and western blot analysis, respectively. (O) Luciferase reporter assay for GES-1 cells transfected with reporter plasmids containing serially truncated ALKBH5 promoter constructs and then treated with 100 μ M for 48 h. (P and Q) The binding sites of p65 on ALKBH5 promoter were identified via ChIP assay. Each experiment was performed in triplicate. * $p < 0.05$, ** $p < 0.01$, *** $p < 0.001$.

MATERIALS AND METHODS

Cell culture and specimens

Human GC cell lines MGC803, MKN28, MKN45, and AGS and gastric epithelial cell line GES-1 were acquired from the Shanghai Institute of Biochemistry and Cell Biology, Chinese Academy of Sci-

ences (Shanghai, China). They were cultured in RPMI 1640 medium (GIBCO BRL, Grand Island, NY, USA).

An IM TMA containing 80 cases (ST8017a, cohort 1) was purchased from Alenabio Biotech (Xi'an, China). Paraffin-embedded samples of

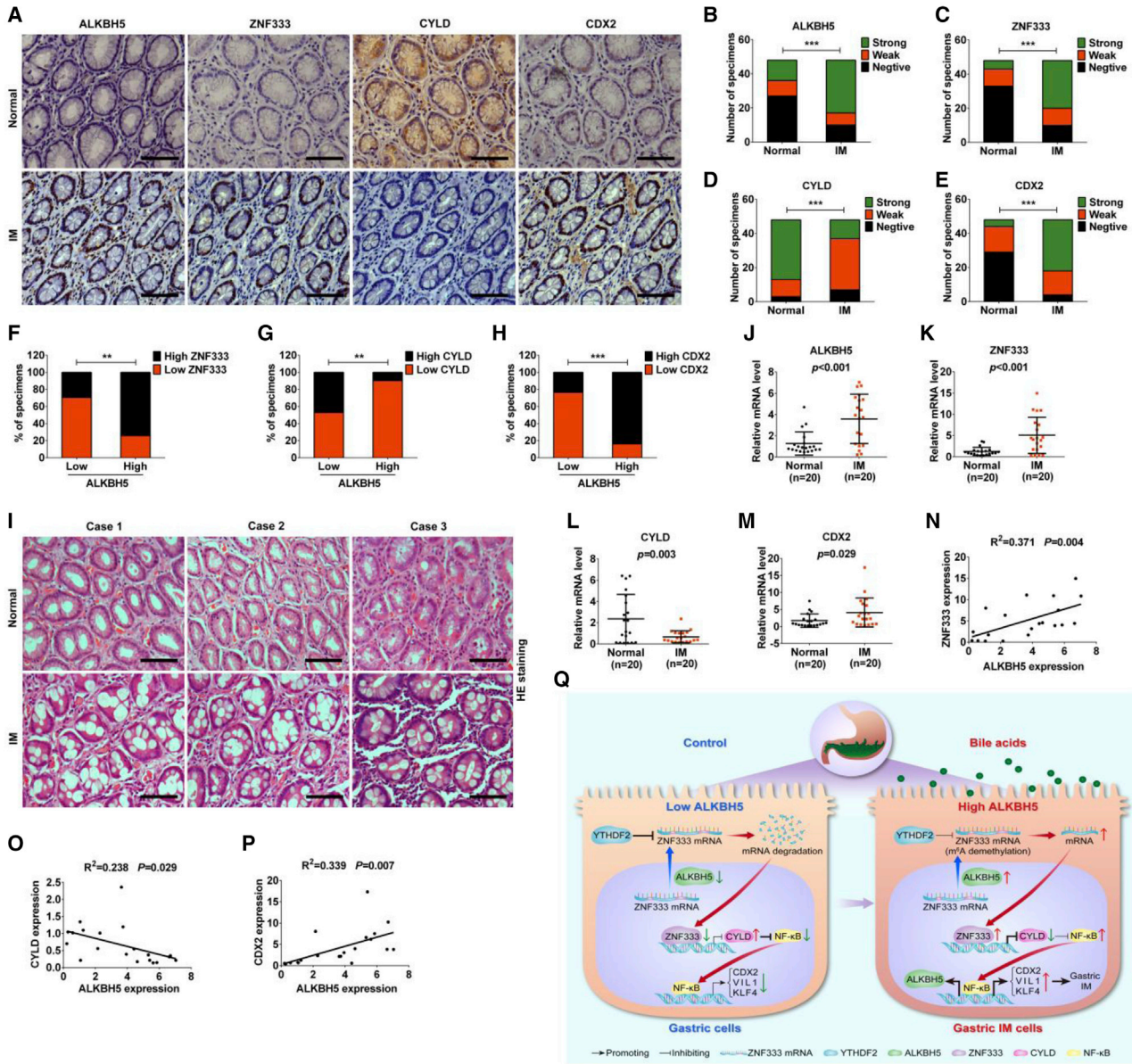


Figure 8. ALKBH5/ZNF333/CDX2 pathway is responsible for gastric IM

(A) Representative IHC staining of ZNF333, CYLD, and CDX2 in pathologic serial sections of gastric IM tissues with low or high ALKBH5 expression. Scale bars: 100 μ m. (B–E) IHC staining analysis for ALKBH5, ZNF333, CYLD, and CDX2 in 48 gastric IM tissues and paired normal tissues (cohort 2). (F) Association between ALKBH5 and ZNF333 levels in 48 gastric IM tissues. (G) Association between ALKBH5 and CYLD levels in 48 gastric IM tissues. (H) Association between ALKBH5 and CDX2 levels in 48 gastric IM tissues. (I) Representative HE staining images of 20 pairs of gastric IM and normal tissues (cohort 3) Scale bars: 100 μ m. (J–M) The mRNA levels of ALKBH5, ZNF333, CYLD, and CDX2 in 20 pairs of gastric IM and normal tissues. (N) Positive correlation between ALKBH5 mRNA level and ZNF333 mRNA level in 20 pairs of gastric IM and normal tissues. (O) Negative correlation between ALKBH5 mRNA level and CYLD mRNA level in 20 pairs of gastric IM and normal tissues. (P) Positive correlation between ALKBH5 mRNA level and CDX2 mRNA level in 20 pairs of gastric IM and normal tissues. (Q) A schematic model of ALKBH5-NF- κ B signaling circuit in gastric IM cells. Bile acid-induced ALKBH5 enhances ZNF333 levels through an m⁶A-YTHDF2-dependent manner. ZNF333 suppresses the expression of CYLD and abrogates its inhibition on NF- κ B signaling. Activation of p65 not only promotes the expression of intestinal markers but also enhances the transcription activity of ALKBH5 in the nucleus, thus forming an m⁶A-associated positive feedforward circuit. ** $p < 0.01$, *** $p < 0.001$.

gastric IM tissues and paired adjacent normal mucosa were obtained from 48 patients (IM 48, normal 48, cohort 2) at Shanghai Renji Hospital. All of the specimens were histopathologically confirmed by two

pathologists. Another 40 RNA samples of IM and paired normal mucosa (IM 20, normal 20, cohort 3) were also collected. This study was approved by the ethics committee of Renji Hospital.

Quantitative real-time PCR and plasmid construction

Quantitative real-time-PCR was conducted as previously described.⁴⁴ The results were normalized to the mRNA expression of human glyceraldehyde-3-phosphate dehydrogenase (GAPDH). For plasmid construction, small interfering RNA (siRNA) specifically targeting CYLD and non-targeting control (si-NC) were synthesized by RiboBio Technology (Guangzhou, China). The control short hairpin RNA (shRNA), ALKBH5 shRNA1/2, ZNF333 shRNA, ALKBH5 overexpressing lentivirus, ZNF333 overexpressing lentivirus, CYLD overexpressing lentivirus, and all plasmids were constructed using OBIO Technology (Shanghai, China). The detailed sequences of primers used are listed in [Tables S3](#) and [S4](#).

IHC

The IHC assay was conducted with antibodies against human ALKBH5 (Abcam), ZNF333 (Invitrogen), CYLD (Abcam), CDX2 (Abcam), or p-p65 (CST). The final staining was divided into three grades (negative, weak, and strong) based on the staining intensity and area.²⁷ The staining intensity was scored as 0 (no staining), 1 (weak), or 2 (strong). The staining area was scored as follows: 0 (\leq 10% positive staining), 1 (11%–25% positive staining), 2 (26%–50% positive staining), 3 (51%–75% positive staining), and 4 (\geq 75% positive staining). Staining intensity and staining area were summed up to give a final total score index: an overall score of \leq 3 was defined as negative expression, of >3 – \leq 6 as weak expression, and of >6 as strong expression. It was also divided into high-expression (strong staining) and low-expression (negative and weak staining) groups.

Confocal immunofluorescence assay

Cells were fixed in 1% formaldehyde for 20 min and permeabilized with Triton X-100 (0.2%) for 5 min. Next, cells were washed 3 times in PBS, blocked for 1 h with 2% BSA, and incubated with primary antibodies specific for ALKBH5 (Abcam), ZNF333 (Invitrogen), p65 (CST), CDX2 (Abcam), VIL1 (Abcam), and KLF4 (Abcam) for 2 h. They were then washed 3 times in PBS and incubated with secondary antibodies for 1 h at room temperature.

Dot blot

After extraction using an RNeasy mini kit, RNA samples were spotted onto a Hybond-N⁺ membrane (GE Healthcare, Chicago, IL, USA) and crosslinked. The membrane was then incubated in blocking buffer for 2 h and with specific anti-m⁶A antibody (Abcam) overnight at 4°C. It was then washed, incubated with an anti-mouse antibody, and washed again. Finally, the membrane was developed using western blotting detection reagent. Methylene blue was used as the loading control.

Luciferase reporter assay

Cells were transfected with luciferase reporter and the indicated expression was constructed in 24-well plates. The activities of firefly luciferase and renilla luciferase in cell extracts were measured 48 h after transfection. Firefly luciferase activities were normalized to those of renilla luciferase. The results were analyzed using a dual-luciferase reporter gene assay system (Promega, Madison, WI, USA).

Western blot

Cell lysates were immunoblotted with primary antibodies targeting ALKBH5 (Abcam), ZNF333 (Invitrogen), CDX2 (Abcam), VIL1 (Abcam), KLF4 (Abcam), YTHDF2 (Abcam), p65 (CST), p-p65 (CST), FLAG (CST), and GAPDH (Abcam). The intensity of the fluorescence was detected using a chemiluminescence system (Amersham Biosciences, Piscataway, NJ, USA), and quantified using Quantity One software (Bio-Rad, USA).

RNA sequencing, m⁶A sequencing, and MeRIP assays

m⁶A and RNA-sequencings were performed using RiboBio Technology (Guangzhou, China). m⁶A antibody immunoprecipitation RNA was quality controlled with QubitTM (Thermo Fisher Scientific, USA) and Agilent 2200 TapeStation (Agilent Technologies, USA). Then, 100 ng RNA was used for library building following the NEB-Next Ultra RNA Library Prep Kit protocol for Illumina (NEB, USA). The final library product was assessed and then sequenced on Illumina platform pair end reads for 150 bp. The clean reads underwent rRNA deleting through RNAcentral to obtain effective reads. Effective reads from input sample can be used for RNA sequencing analysis, the reads count value of each transcript was calculated by HTSeq, and then the FPKM (fragments per kilobase of transcript per million mapped reads) value was estimated. The GO and KEGG analyses with adjusted $p < 0.05$ were considered statistically significant. The m⁶A sequencing and RNA sequencing datasets were submitted to the GEO database under the accession number GSE179185.

The MeRIP assay was performed according to a previously reported protocol.⁴⁵ Poly-A-purified RNA was fragmented and immunoprecipitated with anti-m⁶A antibody (Abcam). Immunoprecipitated RNA was washed, eluted with m⁶A nucleotide solution, purified, and analyzed by quantitative real-time-PCR.

mRNA stability assay

The transcriptional inhibitor actinomycin D was used in this assay. Samples were harvested at different times after treatment with 2 μ M actinomycin D.²⁶ The total RNA was isolated using an RNeasy Plus Mini Kit (QIAGEN, Valencia, CA, USA). Given that HPRT1 mRNA is not modified by m⁶A, is rarely affected by actinomycin D, and is not bound by YTHDF2, the data were normalized to the HPRT1 housekeeping gene.^{19,46}

ChIP assay

ChIP assay was conducted using a ChIP Assay Kit (Millipore, Bedford, MA, USA). Chromatin was immunoprecipitated with specific antibodies. Precipitated DNA samples were purified and analyzed by qPCR. The detailed sequences of primers used for ChIP-PCR are shown in [Table S5](#).

Statistical analysis

For continuous data, Student's *t* test and one-way ANOVA were used to compare differences. Categorical data were compared using the chi-square test. Spearman's correlation was used to assess the correlations between gene expression levels. All of the statistical analyses

were performed using SPSS version 19.0 software (SPSS, Chicago, IL, USA). $p < 0.05$ was considered statistically significant.

SUPPLEMENTAL INFORMATION

Supplemental information can be found online at <https://doi.org/10.1016/j.omtn.2021.08.019>.

ACKNOWLEDGMENTS

This work was supported by The National Natural Science Foundation of China (81802314) and the Interdisciplinary Project Training Fund of Shanghai Jiao Tong University (YG2019QNB20).

AUTHOR CONTRIBUTIONS

E.Z., B.Y., F.Y., and W.J. conceived and designed the project and wrote the manuscript. B.Y., M.W., R.C., and R.Z. performed most of the experiments. C.S. and T.B. collected and analyzed the clinical and pathological data. All of the authors read and approved the final manuscript.

DECLARATION OF INTERESTS

The authors declare no competing interests.

REFERENCES

- Rokkas, T., Filipe, M.I., and Sladen, G.E. (1991). Detection of an increased incidence of early gastric cancer in patients with intestinal metaplasia type III who are closely followed up. *Gut* 32, 1110–1113.
- de Vries, A.C., van Grieken, N.C., Looman, C.W., Casparie, M.K., de Vries, E., Meijer, G.A., and Kuipers, E.J. (2008). Gastric cancer risk in patients with premalignant gastric lesions: a nationwide cohort study in the Netherlands. *Gastroenterology* 134, 945–952.
- Liu, K.S., Wong, I.O., and Leung, W.K. (2016). Helicobacter pylori associated gastric intestinal metaplasia: Treatment and surveillance. *World J. Gastroenterol.* 22, 1311–1320.
- Dixon, M.F., Mapstone, N.P., Neville, P.M., Moayyedi, P., and Axon, A.T. (2002). Bile reflux gastritis and intestinal metaplasia at the cardia. *Gut* 51, 351–355.
- Chen, H.-N., Wang, Z., Li, X., and Zhou, Z.G. (2016). Helicobacter pylori eradication cannot reduce the risk of gastric cancer in patients with intestinal metaplasia and dysplasia: evidence from a meta-analysis. *Gastric Cancer* 19, 166–175.
- Leung, W.K., Lin, S.R., Ching, J.Y., To, K.F., Ng, E.K., Chan, F.K., Lau, J.Y., and Sung, J.J. (2004). Factors predicting progression of gastric intestinal metaplasia: results of a randomised trial on Helicobacter pylori eradication. *Gut* 53, 1244–1249.
- Sun, D., Wang, X., Gai, Z., Song, X., Jia, X., and Tian, H. (2015). Bile acids but not acidic acids induce Barrett's esophagus. *Int. J. Clin. Exp. Pathol.* 8, 1384–1392.
- Ni, Z., Min, Y., Han, C., Yuan, T., Lu, W., Ashktorab, H., Smoot, D.T., Wu, Q., Wu, J., Zeng, W., and Shi, Y. (2020). TGR5-HNF4 α axis contributes to bile acid-induced gastric intestinal metaplasia markers expression. *Cell Death Discov.* 6, 56.
- Yuan, T., Ni, Z., Han, C., Min, Y., Sun, N., Liu, C., Shi, M., Lu, W., Wang, N., Du, F., et al. (2019). SOX2 interferes with the function of CDX2 in bile acid-induced gastric intestinal metaplasia. *Cancer Cell Int.* 19, 24.
- Sun, X., Yang, Q., Rogers, C.J., Du, M., and Zhu, M.J. (2017). AMPK improves gut epithelial differentiation and barrier function via regulating Cdx2 expression. *Cell Death Differ.* 24, 819–831.
- Barros, R., Freund, J.N., David, L., and Almeida, R. (2012). Gastric intestinal metaplasia revisited: function and regulation of CDX2. *Trends Mol. Med.* 18, 555–563.
- Li, T., Guo, H., Li, H., Jiang, Y., Zhuang, K., Lei, C., Wu, J., Zhou, H., Zhu, R., Zhao, X., et al. (2019). MicroRNA-92a-1-5p increases CDX2 by targeting FOXD1 in bile acids-induced gastric intestinal metaplasia. *Gut* 68, 1751–1763.
- Kazumori, H., Ishihara, S., and Kinoshita, Y. (2009). Roles of caudal-related homeobox gene Cdx1 in oesophageal epithelial cells in Barrett's epithelium development. *Gut* 58, 620–628.
- Wong, N.A., Wilding, J., Bartlett, S., Liu, Y., Warren, B.F., Piris, J., Maynard, N., Marshall, R., and Bodmer, W.F. (2005). CDX1 is an important molecular mediator of Barrett's metaplasia. *Proc. Natl. Acad. Sci. USA* 102, 7565–7570.
- Fu, Y., Dominissini, D., Rechavi, G., and He, C. (2014). Gene expression regulation mediated through reversible m⁶A RNA methylation. *Nat. Rev. Genet.* 15, 293–306.
- Barbieri, I., Tzelepis, K., Pandolfini, L., Shi, J., Millán-Zambrano, G., Robson, S.C., Aspris, D., Migliori, V., Bannister, A.J., Han, N., et al. (2017). Promoter-bound METTL3 maintains myeloid leukaemia by m⁶A-dependent translation control. *Nature* 552, 126–131.
- Song, H., Feng, X., Zhang, H., Luo, Y., Huang, J., Lin, M., Jin, J., Ding, X., Wu, S., Huang, H., et al. (2019). METTL3 and ALKBH5 oppositely regulate m⁶A modification of TFE3 mRNA, which dictates the fate of hypoxia/reoxygenation-treated cardiomyocytes. *Autophagy* 15, 1419–1437.
- Zhang, X., Wei, L.H., Wang, Y., Xiao, Y., Liu, J., Zhang, W., Yan, N., Amu, G., Tang, X., Zhang, L., and Jia, G. (2019). Structural insights into FTO's catalytic mechanism for the demethylation of multiple RNA substrates. *Proc. Natl. Acad. Sci. USA* 116, 2919–2924.
- Wang, X., Lu, Z., Gomez, A., Hon, G.C., Yue, Y., Han, D., Fu, Y., Parisien, M., Dai, Q., Jia, G., et al. (2014). N6-methyladenosine-dependent regulation of messenger RNA stability. *Nature* 505, 117–120.
- Bartosovic, M., Molares, H.C., Gregorova, P., Hrossova, D., Kudla, G., and Vanacova, S. (2017). N6-methyladenosine demethylase FTO targets pre-mRNAs and regulates alternative splicing and 3'-end processing. *Nucleic Acids Res.* 45, 11356–11370.
- Edens, B.M., Vissers, C., Su, J., Arumugam, S., Xu, Z., Shi, H., Miller, N., Rojas Ringeling, F., Ming, G.L., He, C., et al. (2019). FMRP Modulates Neural Differentiation through m⁶A-Dependent mRNA Nuclear Export. *Cell Rep.* 28, 845–854.e5.
- Alarcón, C.R., Lee, H., Goodarzi, H., Halberg, N., and Tavazoie, S.F. (2015). N6-methyladenosine marks primary microRNAs for processing. *Nature* 519, 482–485.
- Huang, H., Weng, H., Zhou, K., Wu, T., Zhao, B.S., Sun, M., Chen, Z., Deng, X., Xiao, G., Auer, F., et al. (2019). Histone H3 trimethylation at lysine 36 guides m⁶A RNA modification co-transcriptionally. *Nature* 567, 414–419.
- Tang, C., Klukovich, R., Peng, H., Wang, Z., Yu, T., Zhang, Y., Zheng, H., Klungland, A., and Yan, W. (2018). ALKBH5-dependent m6A demethylation controls splicing and stability of long 3'-UTR mRNAs in male germ cells. *Proc. Natl. Acad. Sci. USA* 115, E325–E333.
- Zhou, J., Wan, J., Shu, X.E., Mao, Y., Liu, X.M., Yuan, X., Zhang, X., Hess, M.E., Brüning, J.C., and Qian, S.B. (2018). N⁶-Methyladenosine Guides mRNA Alternative Translation during Integrated Stress Response. *Mol. Cell* 69, 636–647.e7.
- Yang, S., Wei, J., Cui, Y.H., Park, G., Shah, P., Deng, Y., Aplin, A.E., Lu, Z., Hwang, S., He, C., and He, Y.Y. (2019). m⁶A mRNA demethylase FTO regulates melanoma tumorigenicity and response to anti-PD-1 blockade. *Nat. Commun.* 10, 2782.
- Yue, B., Song, C., Yang, L., Cui, R., Cheng, X., Zhang, Z., and Zhao, G. (2019). METTL3-mediated N6-methyladenosine modification is critical for epithelial-mesenchymal transition and metastasis of gastric cancer. *Mol. Cancer* 18, 142.
- Dang, L.H., Chen, F., Ying, C., Chun, S.Y., Knock, S.A., Appelman, H.D., and Dang, D.T. (2006). CDX2 has tumorigenic potential in the human colon cancer cell lines LOVO and SW48. *Oncogene* 25, 2264–2272.
- Coskun, M., Olsen, A.K., Bzorek, M., Holck, S., Engel, U.H., Nielsen, O.H., and Troelsen, J.T. (2014). Involvement of CDX2 in the cross talk between TNF- α and Wnt signaling pathway in the colon cancer cell line Caco-2. *Carcinogenesis* 35, 1185–1192.
- Zhang, S., Zhao, B.S., Zhou, A., Lin, K., Zheng, S., Lu, Z., Chen, Y., Sulman, E.P., Xie, K., Bögl, O., et al. (2017). m⁶A Demethylase ALKBH5 Maintains Tumorigenicity of Glioblastoma Stem-like Cells by Sustaining FOXM1 Expression and Cell Proliferation Program. *Cancer Cell* 31, 591–606.e6.
- Guo, X., Li, K., Jiang, W., Hu, Y., Xiao, W., Huang, Y., Feng, Y., Pan, Q., and Wan, R. (2020). RNA demethylase ALKBH5 prevents pancreatic cancer progression by

- posttranscriptional activation of PER1 in an m⁶A-YTHDF2-dependent manner. *Mol. Cancer* 19, 91.
32. Yang, Y., Hsu, P.J., Chen, Y.S., and Yang, Y.G. (2018). Dynamic transcriptomic m⁶A decoration: writers, erasers, readers and functions in RNA metabolism. *Cell Res.* 28, 616–624.
 33. Dempersmier, J., Sambeat, A., Gulyaeva, O., Paul, S.M., Hudak, C.S., Raposo, H.F., Kwan, H.Y., Kang, C., Wong, R.H., and Sul, H.S. (2015). Cold-inducible Zfp516 activates UCP1 transcription to promote browning of white fat and development of brown fat. *Mol. Cell* 57, 235–246.
 34. Li, L., Liu, X., He, L., Yang, J., Pei, F., Li, W., Liu, S., Chen, Z., Xie, G., Xu, B., et al. (2017). ZNF516 suppresses EGFR by targeting the CtBP/LSD1/CoREST complex to chromatin. *Nat. Commun.* 8, 691.
 35. Jing, Z., Liu, Y., Dong, M., Hu, S., and Huang, S. (2004). Identification of the DNA binding element of the human ZNF333 protein. *J. Biochem. Mol. Biol.* 37, 663–670.
 36. Grant, C.E., Bailey, T.L., and Noble, W.S. (2011). FIMO: scanning for occurrences of a given motif. *Bioinformatics* 27, 1017–1018.
 37. An, J., Mo, D., Liu, H., Veena, M.S., Srivatsan, E.S., Massoumi, R., and Rettig, M.B. (2008). Inactivation of the CYLD deubiquitinase by HPV E6 mediates hypoxia-induced NF-kappaB activation. *Cancer Cell* 14, 394–407.
 38. Espinosa, L., Cathelin, S., D'Altri, T., Trimarchi, T., Statnikov, A., Guiu, J., Rodilla, V., Inglés-Esteve, J., Nomdedeu, J., Bellosillo, B., et al. (2010). The Notch/Hes1 pathway sustains NF-kB activation through CYLD repression in T cell leukemia. *Cancer Cell* 18, 268–281.
 39. Huo, X., Zhang, X., Yu, C., Cheng, E., Zhang, Q., Dunbar, K.B., Pham, T.H., Lynch, J.P., Wang, D.H., Bresalier, R.S., et al. (2018). Aspirin prevents NF-kB activation and CDX2 expression stimulated by acid and bile salts in oesophageal squamous cells of patients with Barrett's oesophagus. *Gut* 67, 606–615.
 40. Chen, L., Toke, N.H., Luo, S., Vasoya, R.P., Fullem, R.L., Parthasarathy, A., Perekatt, A.O., and Verzi, M.P. (2019). A reinforcing HNF4-SMAD4 feed-forward module stabilizes enterocyte identity. *Nat. Genet.* 51, 777–785.
 41. Lian, H., Wang, Q.H., Zhu, C.B., Ma, J., and Jin, W.L. (2018). Deciphering the Epitranscriptome in Cancer. *Trends Cancer* 4, 207–221.
 42. Tian, Y., Breedveld, G.J., Huang, S., Oostra, B.A., Heutink, P., and Lo, W.H. (2002). Characterization of ZNF333, a novel double KRAB domain containing zinc finger gene on human chromosome 19p13.1. *Biochim. Biophys. Acta* 1577, 121–125.
 43. Asano, N., Imatani, A., Watanabe, T., Fushiya, J., Kondo, Y., Jin, X., Ara, N., Uno, K., Iijima, K., Koike, T., et al. (2016). Cdx2 Expression and Intestinal Metaplasia Induced by H. pylori Infection of Gastric Cells Is Regulated by NOD1-Mediated Innate Immune Responses. *Cancer Res.* 76, 1135–1145.
 44. Yue, B., Qiu, S., Zhao, S., Liu, C., Zhang, D., Yu, F., Peng, Z., and Yan, D. (2016). LncRNA-ATB mediated E-cadherin repression promotes the progression of colon cancer and predicts poor prognosis. *J. Gastroenterol. Hepatol.* 31, 595–603.
 45. Vu, L.P., Pickering, B.F., Cheng, Y., Zaccara, S., Nguyen, D., Minuesa, G., Chou, T., Chow, A., Saletore, Y., MacKay, M., et al. (2017). The N⁶-methyladenosine (m⁶A)-forming enzyme METTL3 controls myeloid differentiation of normal hematopoietic and leukemia cells. *Nat. Med.* 23, 1369–1376.
 46. Du, H., Zhao, Y., He, J., Zhang, Y., Xi, H., Liu, M., Ma, J., and Wu, L. (2016). YTHDF2 destabilizes m(6)A-containing RNA through direct recruitment of the CCR4-NOT deadenylase complex. *Nat. Commun.* 7, 12626.